Available online at www.sciencedirect.com
SCIENCE DIRECT®
Journal of Power Sources 139 (2005) 126–140
JOURNAL OF POWER SOURCES
www.elsevier.com/locate/jpowsour

Integrated thermal engineering analyses with heat transfer at periphery of planar solid oxide fuel cell

Yau-Pin Chyou[a,*], Tsang-Dong Chung[b], Jong-Sheng Chen[a], Ri-Fong Shie[a]

[a] *Environmental and Energy Technology Center, Institute of Nuclear Energy Research (INER), P.O. Box 3-14, 1000, Wenhua Road, Chiaan Village, Lung-Tan 325, Tao-Yuan, Taiwan, ROC*
[b] *Nanya Institute of Technology, 414, Sec. 3, Chung-Shang E. Rd., Chung-Li 320, Tao-Yuan, Taiwan, ROC*

Received 12 May 2004; accepted 30 June 2004
Available online 11 September 2004

Abstract

This paper focuses on the thermal engineering design and analysis of solid oxide fuel cell (SOFC) units, with emphasis on cell performance and component design. In engineering practice, insulation materials would be deployed as the enclosure of an SOFC stack to reduce the heat loss to the environment. In this work, a computational methodology has been implemented to characterize the thermal engineering performance of a planar SOFC. The present calculation procedure integrates the steady-sate electrochemical reactions of the SOFC with finite-element models for thermo-mechanical analyses of the interconnect through iteration processes, so that a unified temperature distribution with heat loss effect can be obtained. Present results show that the convergent rate of the adopted methodology is quite efficient, and that the temperature patterns are compatible with those reported in the literature. Furthermore, this work has also developed a bulk heat-transfer model for simplified design analysis. The concept of total heat resistance is employed to facilitate the one-dimensional (1D) analyses and to determine the predominant parameters that affect heat-transfer behaviour. Moreover, some accommodation factors have been deduced to correlate the 1D results of lateral heat transfer with those of two-dimensional (2D) finite-element analyses, as this will be beneficial for rapid prototyping processes.

Keywords: Solid oxide fuel cell; Thermal engineering practice; Electrochemical model; Finite element analysis; Heat-transfer mechanism; Thermal insulation

1. Fundamentals and approach

Among the various types of fuel cell, the solid oxide fuel cell (SOFC) belongs to the high-temperature category; its operating temperature ranges from about 600 to 1000 °C. The working principle of the SOFC is illustrated schematically in Fig. 1. Fuel is fed into the anode side, while on the opposite cathode side, air is typically utilized as the oxidant. The oxidant generates O^{2-} ions that serve as charge carriers through the electrolyte to the anode, where they react with fuel to release electrons. By guiding electrons via an outer electric-conducting loop back to the anode, this device generates direct current (dc) electricity. One of the major advantages of the SOFC is its fuel flexibility. For example, the fuel can be a mixture consisting of hydrogen (H_2), carbon monoxide (CO), methane (CH_4) and even some higher hydrocarbons. This feature avoids the expense of producing hydrogen of high purity that is demanded by low-temperature fuel cells.

The basic cell consists of a positive electrode (cathode)–electrolyte–negative electrode (anode) (PEN) assembly and two end-plates, with piping on each side. Flow channels for fuel and oxidant are integrated on the end plates at the anode and cathode sides, respectively. In practical applications, multiple cells are piled up to form a stack that corresponds to serial connections of the electric loop for an individual cell. In this case, interconnects with double-sided flow channels will lay between the PENs. A scheme of a stack assembly is shown in Fig. 2.

To design and optimize a stack configuration, it is necessary to establish analytical tools for simulating the

* Corresponding author. Tel.: +886 3 471 1400x6614; fax: +886 3 471 1409.
E-mail address: chyouy@asme.org (Y.-P. Chyou).

0378-7753/$ – see front matter © 2004 Elsevier B.V. All rights reserved.
doi:10.1016/j.jpowsour.2004.07.001

Nomenclature

Symbols

A	contact area in channel for convection
C	molar flow rate
C_p	specific heat
F	Faraday constant
G	Gibbs function
Gr	Grashof number
g	gravity
H	height of channel
h	heat-transfer coefficient
I	current
k	thermal conductivity
L	characteristic length
Nu	Nusselt number
P	pressure
Pr	Prandtl number
Q	heat source
q	heat flux per unit surface
R	gas constant, heat resistance
Re	Reynolds number
T	temperature
U	total heat-transfer coefficient
u	velocity
V	voltage
W	width of channel
X	thickness

Greek letters

β	coefficient of expansion
Δ	difference
ν	kinematic viscosity
λ	oxygen to water ratio

Subscripts and superscripts

0	standard state
a	air
act	activation
con	concentration
f	fuel
i	species
L	characteristic length
m	mean
nst	Nernst
o	outer
ohm	ohmic
op	operation state
pol	polarization
s	solid
x	x direction
y	y direction
w	wall

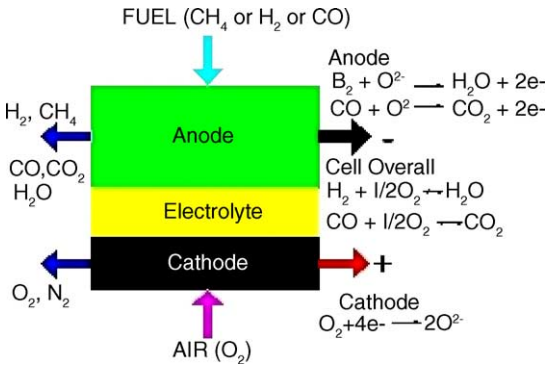

Fig. 1. Schematics of operating principles of a SOFC.

cell performance. Reports of the modelling of planar SOFCs have been increasing during the past few years, and most of these have dealt with steady operation. Some previous studies will be briefly reviewed here to illustrate the evolution of modelling developments. Pioneer work [1] examined a three-dimensional (3D) model for steady and load-following operations to analyze the cell characteristics as well as the distribution of temperature, current density and gas species under the influence of various parameters. The basic assumptions included uniform flow in the cell, no pressure drop and adiabatic conditions on the periphery of stack. These have been adopted in some later studies. Iwata et al. [2] investigated the effects of fuel re-circulation ratio, operating pressure, flow configuration and thermal boundary conditions on the distribution of temperature and current density. The conservation equations were written in discretized forms for cell elements, which were arranged periodically in span-wise direction to complete a unit cell. Similar assumptions as those in [1] were implemented. In addition, each segmented cell was assumed to have one representative temperature and an additional option of a radiation boundary could be set at the upper and lower surfaces.

Some investigators have employed commercial computational fluid dynamics (CFD) codes to perform thermofluid analyses of planar cells, in which the computational domain has been focused on either flow channels [3,4] or cell components [5]. For example, Yakabe et al. [3] presented the distribution of chemical species, temperature, potential and current density in flow channels of a planar SOFC. Their model was based on a simplified single-unit cell with a parallel flow pattern and a finite volume that simulated half of the repeating unit located in the middle part of a one-cell stack. The thermal boundaries employed adiabatic and cyclic conditions at the edges and the surfaces connecting to the adjacent units in a span-wise direction, respectively. For the sake of simplicity, radiation losses were neglected in the steady-state energy equation, and the diffusion overpotential was also omitted in the discrete electrochemical model (ECM). Formulae for radiant heat-exchange inside the channels were derived in follow-up work but were implemented only for one calculating condition because of the amount of time required, which

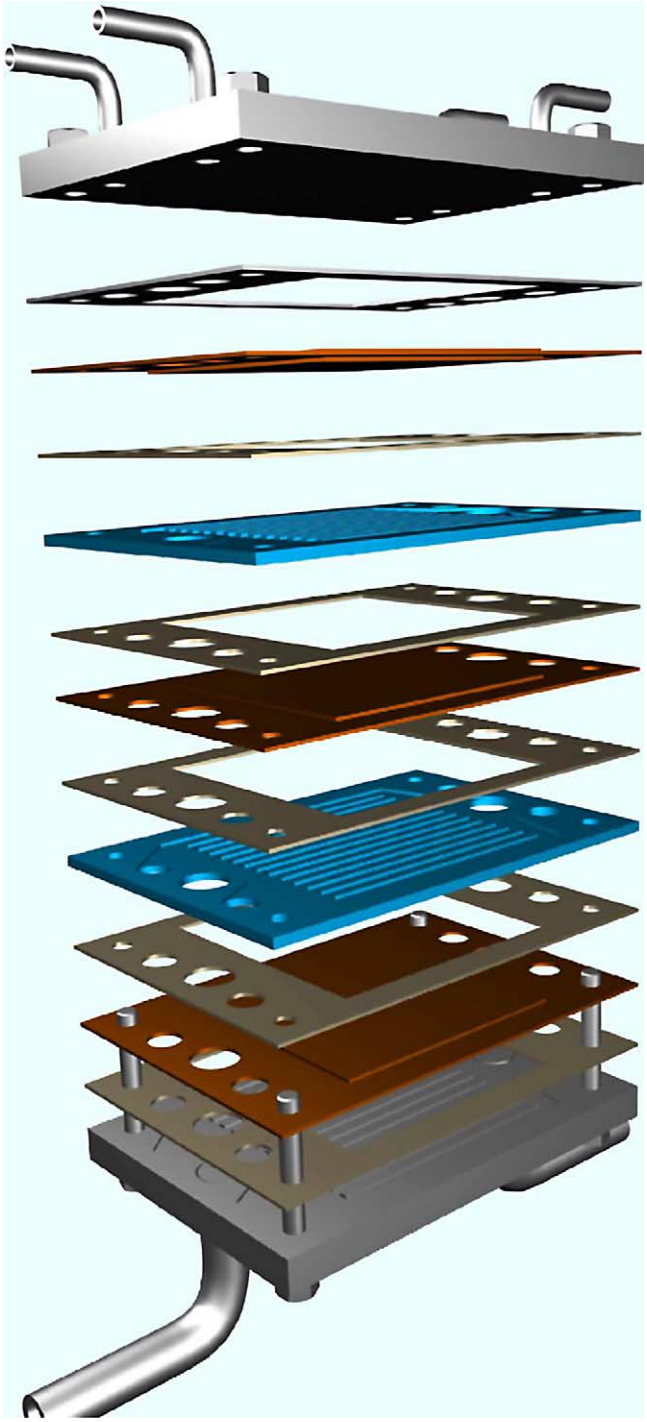

Fig. 2. Schematics of SOFC stack assembly.

turned out to be 10 times that of the non-radiant counterpart. The effect of radiation has been considered to be small, however, due to the large aspect ratio of the flow channels [4].

An alternative approach was presented by Recknagle et al. [5], in which 3D model geometries, including internal manifolds, PENs, interconnects and glass seals, were created to simulate generic stack designs, either for cross- or parallel-flow configurations. Individual flow channels created by webs in the interconnect were not modelled; instead, the region was assumed to be one large flow passage. The effect of radiation was perceived to be small relative to the other modes of heat transfer and was neglected. Cyclic boundary conditions were imposed at the top and bottom of the model domains, while the lateral walls were assumed to be adiabatic. The above thermo-fluid model was combined with a unit-cell electrochemistry model to form a simulation tool for a planar SOFC.

Due to the high operating temperature of SOFCs, heat loss to the environment becomes inevitable and, in turn, will affect the overall system performance. Heat transfer across the walls at the periphery of the stack is hard to estimate, however, so that this type of thermal boundary has been ignored in the energy equation in many reports of the characterization of cell performance, including electrochemical, thermal and flow aspects. As mentioned by some investigators, it is difficult to determine the exact boundary at the edge parts. Hence, all the aforementioned studies have employed adiabatic boundaries for the energy equation on the periphery of the computational domain, regardless of flow channels or cell components.

In this work, an efficient computational methodology is proposed to deal with the behaviour discussed above, of which the procedures and some preliminary results have been presented to local and international scientific communities [6,7]. At present, a computer code for analyzing the steady-sate electrochemical reactions has been developed, by which the characteristics of SOFC can be calculated. On the other hand, finite-element models for thermo-mechanical analyses of an interconnect with an insulation envelope have also been established. Hence, combined electrochemical and heat-transfer analyses can be executed through an iteration process from both tools, and a unified temperature distribution with a heat loss effect can be obtained. The results show that the convergent rate of the above methodology is quite efficient, and that the temperature patterns are compatible with counterparts reported in the literature.

2. Cell performance evaluation

This section concerns mainly with the characteristics of the SOFC, as well as thermal, flows and electric parameters through electrochemical reactions. Detailed description on the computational procedure and the effects of various parameters has been documented elsewhere [8].

2.1. Electrochemical computation

Basically, a fuel cell is an electrochemical reactor that converts chemical energy to electrical energy. The reactions at the anode and the cathode of a SOFC that operates on hydrogen and oxygen are as follows:

$$\text{at anode}: \quad H_2 + O^{2-} \rightarrow H_2O + 2e^- \tag{1}$$

$$\text{at cathode}: \quad \tfrac{1}{2}O_2 + 2e^- \rightarrow O^{2-} \tag{2}$$

The Nernst potential V_{nst} from chemical reactions can be expressed by:

$$V_{nst} = -\frac{\Delta G^{\circ}}{2F} + \frac{RT}{2F} \ln\left(\frac{P_{H_2} P_{O_2}^{1/2}}{P_{H_2O}}\right) \quad (3)$$

where ΔG° is the Gibbs free energy; F the Faraday constant; R the gas constant; and P_{H_2}, P_{O_2} and P_{H_2O} are the partial pressures of H_2, O_2 and H_2O, respectively. The aforementioned potential is a function of fuel composition, and internal reforming of methane will be considered in this work.

In fact, the actual operating voltage, V_{op}, of a cell will be lower than the theoretical value of V_{nst}, due to the external connector and the internal resistance of the PEN. The potential drop within the cell loop considered in the present model includes: (i) ohmic overpotential, (ii) concentration overpotential and (iii) activation overpotential [2,9–12]. Detailed formulations of these overpotentials have been documented previously [8], i.e.,

$$V_{op} = V_{nst} - V_{pol} \quad (4)$$

$$V_{pol} = V_{ohm} + V_{act} + V_{con} \quad (5)$$

The chemical reactions between the hydrogen-rich gas and the oxidant are the major mechanisms that govern the energy and mass conservations in the cell. For a natural gas (NG) fed SOFC, the following reactions are included in the electrochemical model and are also shown in Fig. 1.

$$CH_4 + H_2O \rightarrow 3H_2 + CO \quad (6)$$

$$CO + H_2O \rightarrow CO_2 + H_2 \quad (7)$$

$$H_2 + \tfrac{1}{2}O_2 \rightarrow H_2O \quad (8)$$

$$CO + \tfrac{1}{2}O_2 \rightarrow CO_2 \quad (9)$$

Reaction (6) is the reforming process of steam with methane, and is endothermic. The others are exothermic reactions. The heat values vary with temperature and can be calculated from the enthalpies of the reactants and the products. Reliable and comprehensive thermodynamic data for this work were obtained from the JANAF tables [13]. These reactions also govern the mass conservations of the related chemical species.

2.2. Thermal model

Based on energy conservation relations, various temperatures involved in the present model can be calculated, e.g., solid temperature T_s, fuel temperature T_f, and air temperature T_a. A control volume is shown in Fig. 3 and includes fuel, solid and air units for the thermal model, and outlines the relationships among heat fluxes and source terms. Considering conduction through the channel wall and convection with flow, the governing equations for the fluid temperatures can be formulated with the source terms from the chemical

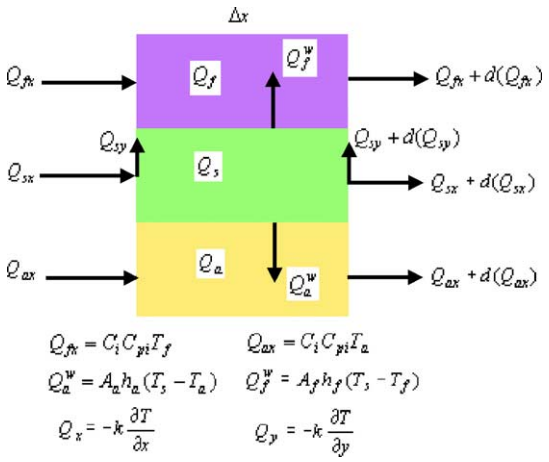

Fig. 3. Control volume of SOFC thermal model.

reactions, i.e.,

$$\sum_i \frac{\partial (C_i C_{pi} T_f)}{\partial x} dx - A_f h_f (T_s - T_f) = Q_f \quad (10)$$

$$\sum_i \frac{\partial (C_i C_{pi} T_a)}{\partial x} dx - A_a h_a (T_s - T_a) = Q_a \quad (11)$$

In Eqs. (10) and (11), C, C_p, A and h represent molar flow rate, specific heat, contact area and heat-transfer coefficient, respectively. Moreover, the subscripts i, f, s and a indicate species i, fuel, solid and air, respectively.

Similarly, the governing equation for solid temperature can be expressed in terms of conduction, convection and source terms, while the last category includes chemical energy from the reactions and the Joule heating term [10], namely:

$$k_x \frac{\partial^2 T_s}{\partial x^2} V_{cv} + k_y \frac{\partial^2 T_s}{\partial y^2} V_{cv} - A_f h_f (T_s - T_f) - A_a h_a (T_s - T_a) = Q_s \quad (12)$$

in which k is the thermal conductivity of the solid, $V_{cv} = \Delta x \Delta y \Delta z$, and the source term is:

$$Q_s = -Q_f - Q_a - I(V_{nst} - V_{ohm} - V_{act} - V_{con}) \quad (13)$$

To circumvent time-consuming and cost-intensive computational fluid dynamics efforts to model convection behaviour, empirical correlations for heat-transfer coefficients were implemented instead. For a rectangular channel, the Nusselt number, Nu, changes with the cross-sectional aspect (width-to-height, W:H) ratio [14]. In preliminary investigations, the value of W:H was selected to be around 2.5 and 3. Hence, the value of 4 for the Nusselt number was adopted to calculate the heat-transfer coefficients for the fuel and air sides.

Table 1
Inlet and outlet conditions of SOFC

	Fuel		Air	
	Inlet	Outlet	Inlet	Outlet
Flow rate (mol h^{-1} per cell)	1.20	1.61	20.00	19.61
Flow rate (mol h^{-1} per stack)	1.20 × 38	1.61 × 38	20.00 × 38	19.61 × 38
Composition (%)				
CH_4	17.1	0.11	/	/
H_2O	49.34	61.27	/	/
H_2	26.26	20.51	/	/
CO	2.94	3.43	/	/
CO_2	4.36	14.68	/	/
N_2	/	/	79.00	80.57
O_2	/	/	21.00	19.43
S/C	2.89		/	
O_2/H_2O	/		7.09	
Temperature (°C)	640	773	640	763
Utilization(%)	66.53		9.28	

2.3. Boundary conditions and computation procedures

It is important that the early stage of research and development is compatible with the state-of-the-art, in order to understand the existing status of technology progress, and to benchmark the results with those that have been reported in the literature. Hence, this work has adopted the '30% prereforming NG' reported by Lehnert et al. [15] as the inlet conditions of the SOFC, for which the compositions are listed in Table 1.

To simplify the analysis model, this work implemented an idealized and bulk approach to handle the boundary conditions in the reaction zones. It has been reported that the pressure loss in a straight type of flow channel is usually less than 5%; hence, this effect is ignored in the present model. In addition, local distribution of the flow field is ignored, and mean values of flow speed estimated from the gas-flow rates are adopted instead in the reaction zones. Furthermore, the adiabatic temperature distribution is first calculated from chemical reactions, and then the effect of heat loss to the environment is then evaluated (see Section 3.3) by combining thermal analysis of the interconnect via a finite element model (FEM).

The above electrochemical and thermal models provide the infrastructure of the integrated SOFC analyses, which are implemented into an indigenous two-dimensional (2D) numerical code. The solution procedure includes several steps, namely:

(i) specification of inlet flow conditions;
(ii) specification of geometry, materials, electric parameters, etc.;
(iii) estimation of initial temperature distributions for solid, fuel and air;
(iv) specification of current density to calculate the operating voltage;
(v) utilization of the Newton–Raphson equation to perform electrochemical computations;
(vi) evaluation of the source terms and heat-transfer coefficients for the energy equations;
(vii) application of the finite-volume method to calculate temperature distributions;
(viii) comparison of the results with the given counterparts, and implementation of iterative processes until convergent criteria are reached.

3. Thermal analyses of the interconnect

The interconnect in a SOFC stack provides several major functions; namely: (i) flow passages for working media through reaction zones; (ii) an electric conductor for a serial loop; and (iii) structural component for pile assembly. Due to the above functional requirements, it is desirable to perform thermo-mechanical analyses for the interconnect in order to ensure its durability and mechanical integrity. The early stage of planning for this issue has been focused on establishing a finite element model and a computational procedure [16].

3.1. Finite element model

As shown in Fig. 2, the present interconnect design is a rectangular plate with a length of 136 mm, a width of 95 mm and a thickness of 3 mm. Flow channels are embedded in the central region of the plate. These provide passages for fuel and oxidant and are subjected to a thermal load. To reduce heat loss to the environment and the outer temperature of the SOFC, the unit is enclosed by two-layered insulation materials. The basic configuration consisted of a 10-mm inner layer of ceramic fibre and a 75-mm ceramic plate as the outer insulation.

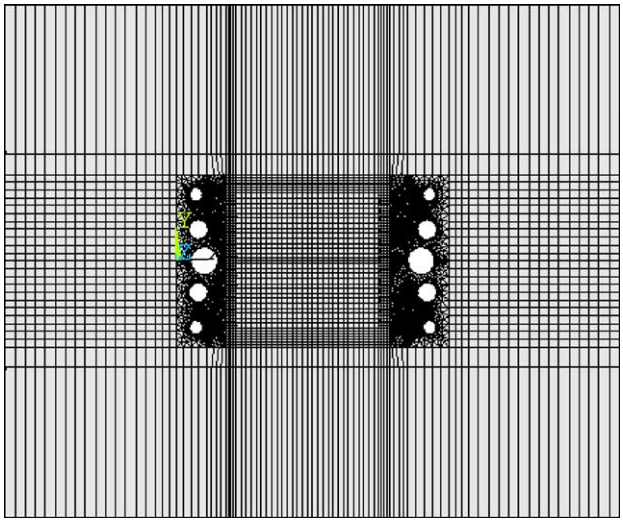

Fig. 4. Finite element model of interconnect with thermal insulations.

Based on the above dimensions of the interconnect and the insulation layers, a finite element model has been established by using the generic computer-aided engineering (CAE) code of ANSYS [17]. This solid model has been built up with the SOLID70 element, and includes 9760 and 574 elements for the interconnect and the insulation layers, respectively. The finite element model of the interconnect with thermal insulation layers is presented in Fig. 4, and the 3D mesh of the interconnect is shown in Fig. 5.

The provisional interconnect was made of Incoloy-800. The material properties are documented in [16] and the thermal conductivity at 800 °C (i.e., k_1 = 25 W m^{-1} °C^{-1}) was adopted in the present analysis. In addition, constant values of thermal conductivity were used for the insulation, i.e., k_2 = 0.198 W m^{-1} °C^{-1} for the inner ceramic fibre and k_3 = 0.215 W m^{-1} °C^{-1} for the outer ceramic plate. The surrounding temperature was assumed to be 40 °C.

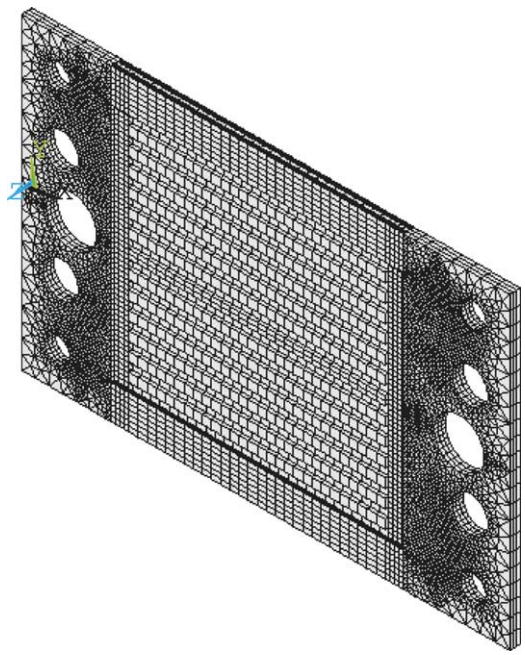

Fig. 5. 3D finite element model of interconnect.

3.2. Two-dimensional heat-transfer analysis

Based on the calculated results in Section 2, the temperature distribution has a 2D nature in the reaction zones. Hence, the corresponding heat-transfer behaviour in the interconnect will exhibit 2D features as well. In practice, the stack is enveloped by insulation materials of low thermal conductivity to diminish the heat loss to the environment and the temperature at the outer edges. Accordingly, the thermal-transport mechanism within the solid parts is dominated by heat conduction and this substantially relieves the demand of CFD efforts. At the outer boundary of the insulation envelop, heat transfer is governed by natural convection to the surroundings. Due to relatively lower temperatures in this region, the effect of local gradients is minimal; hence, heat-transfer coefficients are estimated by taking the average temperature. This simplified approach should pose only a minor influence on the heat-transfer behaviour in the cell core.

In summary, heat-transfer phenomena at the interconnect can be simplified to ‘quasi-conduction’ analyses, for which solutions are directly calculated by utilizing thermal elements embedded in the CAE code. The benefits of this approach are two-fold. On one hand, the temperature distribution at the interconnect can be determined and the necessary boundary conditions for subsequent thermal stress analysis can be obtained. On the other hand, the amount of heat loss can be evaluated and fed back to the ECM for further evaluation and the effect of insulation thickness can also be studied.

3.3. Iteration between FEM and ECM

The integrated thermal analyses of a planar SOFC were divided into two stages. First, the temperature distribution at the reaction zone of the interconnect was evaluated via ECM under adiabatic conditions, and was utilized as the thermal boundary for the FEM. Second, 2D heat-transfer analysis was performed to obtain the overall thermal parameters. These included a heat-loss term that was later fed back to the cell performance evaluation for a more realistic consideration. Through several iterative calculation processes, a unified temperature distribution could be obtained. Details of the calculation procedure and related parametric data have been reported elsewhere [6].

The flow chart of the solution procedure is presented in Fig. 6. At the first step, the adiabatic boundary condition is implemented for the electrochemical calculations in the reaction zone until a convergent solution is achieved. Then, the FEA is activated. The primary adiabatic solu-

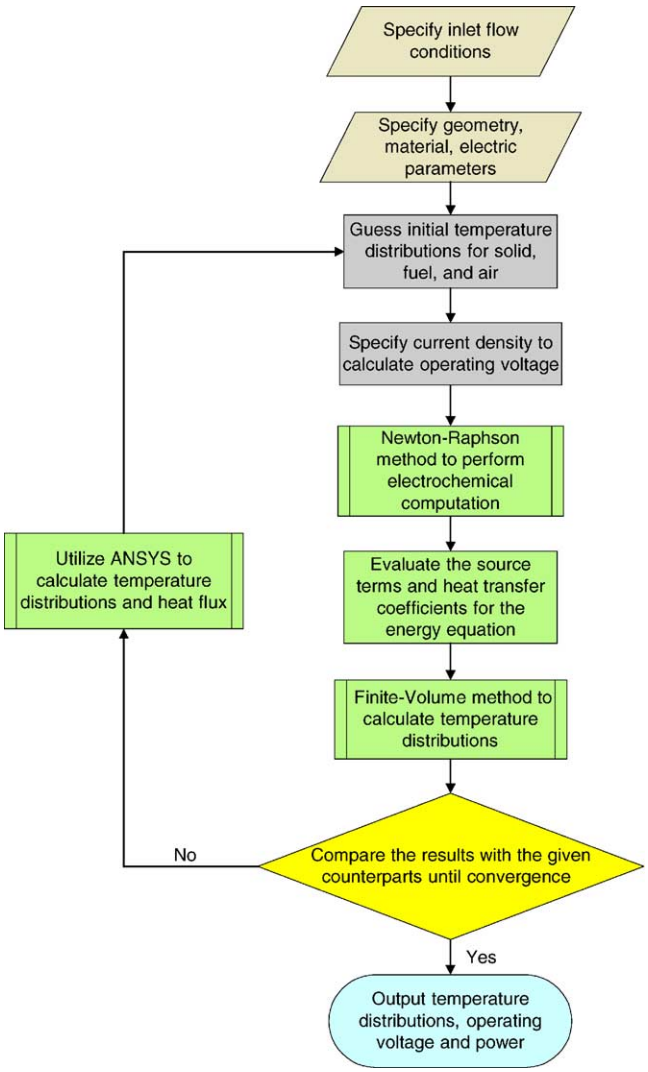

Fig. 6. Flowchart of SOFC electrochemical model.

tion is utilized as the boundary condition for heat-transfer computation in the second step. Iterations between electrochemical and heat-transfer analyses are then performed until convergence.

4. Model for design analysis

The models described above provide the basis for integrated thermal analyses of a planar SOFC. It would be favourable, however, to develop simplified design analysis tools for component prototyping, prior to employing comprehensive finite element analyses. For example, the interconnect is an important structural component of SOFC stacks and its thermal characteristics are essential for subsequent analyses of mechanical integrity in long-term operation. Based on the geometry and sizing of the flow channels on the interconnect, some crucial features of heat-transfer behaviour in the SOFC will be outlined, and a model for design analysis will also be illustrated.

4.1. Bulk heat-transfer model

The approach here is to implement the logics of theoretical analyses, i.e., first to clarify the relationship among various heat-transfer mechanisms via related empirical correlations, then to perform one-dimensional (1D) analytical solutions with bulk values. In the overall model, the heat source originates from the hot gas temperature in the reaction zones; while the heat flux is conveyed to the channel walls through forced convection, and to the edges of the interconnect via conduction. Heat transfer through the insulation layers around the stack is also governed by conduction, and to the environment by natural convection.

Hence, the governing equation of heat flux can be expressed as follows:

$$q = h_i(T_i - T_{w1}) = k_1\frac{T_{w1} - T_{w2}}{\Delta X_1} = k_2\frac{T_{w2} - T_{w3}}{\Delta X_2} = k_3\frac{T_{w3} - T_{w4}}{\Delta X_3} = h_o(T_{w4} - T_\infty). \quad (14)$$

where the subscripts 1, 2 and 3 for k and ΔX represent the interconnect, the inner insulation and the outer layer, respectively; T_i and T_∞ are the fluid temperature inside the channels and the outer surroundings, respectively; and T_{w1} to T_{w4} are the wall temperatures at the edges of solid parts.

Introducing the concept of total heat resistance, Eq. (14) can be rewritten as follows:

$$Q = UA\Delta T = \frac{A\Delta T}{\sum R} = \frac{A\Delta T}{(1/h_i) + (\Delta X_1/k_1) + (\Delta X_2/k_2) + (\Delta X_3/k_3) + (1/h_0)} \quad (15)$$

where U is the total heat-transfer coefficient; A the total heat-transfer area; $\sum R$ the total heat resistance; and $\Delta T = T_i - T_\infty$.

4.2. Correlations of forced convection

The reaction zones of a planar SOFC consist of a series of parallel flow channels. Thus, the heat-transfer behaviour from the internal source to the environment may be regarded as laminar flow over a flat plate, from a global viewpoint. Forced convection phenomena can be simulated with empirical correlations documented in the literature [18].

For external flow over a flat plate, the mean Nusselt number that governs the heat-transfer behaviour normal to the plate can be correlated to the Reynolds number, Re, and the Prandtl number, Pr, in the following expression:

$$Nu_{m,i} = \frac{h_i L}{k_i} = 0.664 Re^{1/2} Pr^{1/3} \quad (16)$$

where

$$Re = \frac{uL}{\nu} \tag{17}$$

In the above equations, k_i, Pr and ν denote the thermal conductivity, Prandtl number and kinematic viscosity of the fluid, respectively. In addition, L is the characteristic length of the flow field and u is the averaged velocity. Hence, the heat-transfer coefficient for forced convection h_i can be calculated.

The Nusselt number will approach a constant value for internal flow, provided that a fully-developed flow condition is achieved. Two types of flow configuration will be illustrated in the following. The first case (Nu_1) is concerned with flow confined by two plates, one of which is adiabatic. The second example (Nu_2) deals with heat transfer through the channel walls, i.e., confined flow. The former governs the heat-transfer behaviour normal to the plate, i.e., similar to that given by Eq. (16), which should be appropriate in discussing the situation at the end plates; while the latter deals with 'all-around' heat flux through a confined channel, which might be utilized to simulate the lateral heat flux at the periphery of the cell. As mentioned earlier, Nu_2 for a rectangular channel changes with the cross-sectional W:H ratio; nevertheless, the values listed in the literature deviate only slightly. Hence, the value of Nu_2 given in the textbook written by Ozisik [18] will be adopted here, for easier reference purposes, for the design analysis model.

The correlations are listed here for further discussion. Since the flow rate of air is substantially larger than that of the fuel, heat-transfer coefficients in the air channels will be implemented in the 1D simplified analyses, as a more conservative approach.

$$Nu_1 = 5.385 \quad \text{for flow between plates (one side adiabatic)} \tag{18}$$

$$Nu_2 = 3.68 \quad \text{for flow confined in channel} \tag{19}$$

4.3. Correlations of natural convection

Natural convection phenomenon can be simulated with the following correlation.

$$Nu_{m,o} = \frac{h_o L}{k_o} = 0.514(Gr_L Pr)^{0.25} \tag{20}$$

where

$$Gr_L = \frac{g\beta(T_{w4} - T_\infty)L^3}{\nu^2} \tag{21}$$

$$\beta = \frac{1}{T_f} = \frac{2}{T_{w4} + T_\infty} \tag{22}$$

In the above equation, k_o is the thermal conductivity of the ambient atmosphere; hence, the heat-transfer coefficient for natural convection h_o can be calculated.

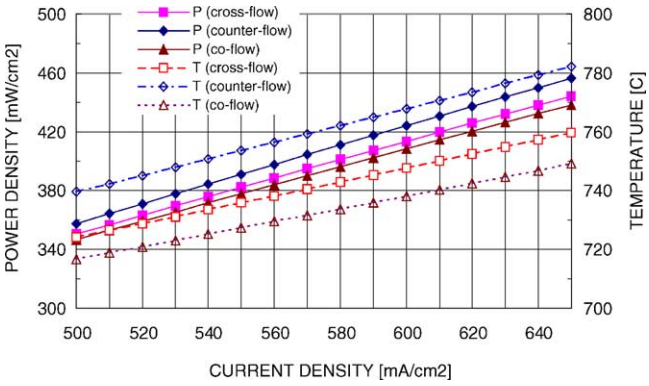

Fig. 7. Comparison of cell performance.

5. Results and discussion

5.1. Cell performance

5.1.1. Influence of flow arrangement

There are usually three types of flow arrangement for a planar SOFC, i.e., co-flow, counter-flow and cross-flow. Cell characteristics will be affected by different flow patterns. A comparison of power density and temperature for various flow arrangements under the same inlet conditions is given in Fig. 7. It is seen that the counter-flow arrangement results in the highest power density and temperature, which is the primary configuration studied in this paper.

Further details of temperature patterns in the active area of a cell with various flow arrangements are revealed in Fig. 8. For simplicity, an adiabatic condition is applied at the boundaries of the computation domain, which might affect the temperature contours near the periphery but would not distort the generic feature in the core area. It is seen that the cross-flow configuration generated a hot island near the fuel inlet and the air outlet in the reaction zone, as shown in Fig. 8a. More uniform temperature distributions can be obtained with parallel-flow configurations. The temperature pattern of the counter-flow configuration is shown in Fig. 8b, while the counterpart of the co-flow case is given in Fig. 8c. These two cases display a similar pattern, i.e., the temperature increases along the airflow direction; but differ in terms of temperature gradient and level. In summary, the outcome obtained from the ECM in this work is qualitatively consistent with that reported in the literature, e.g. [5].

5.1.2. Electrochemical characteristics of SOFC

One of the major considerations in this work has been the utilization of metal rather than ceramics as the material for the interconnect, in order to reduce cost as well as to enhance mechanical integrity and durability. Hence, it has been set in the project specifications that the maximum metal temperature should be kept below or around 800 °C. Through several trial calculations with the ECM described in Section 2, the inlet temperature of 640 °C roughly complies with the

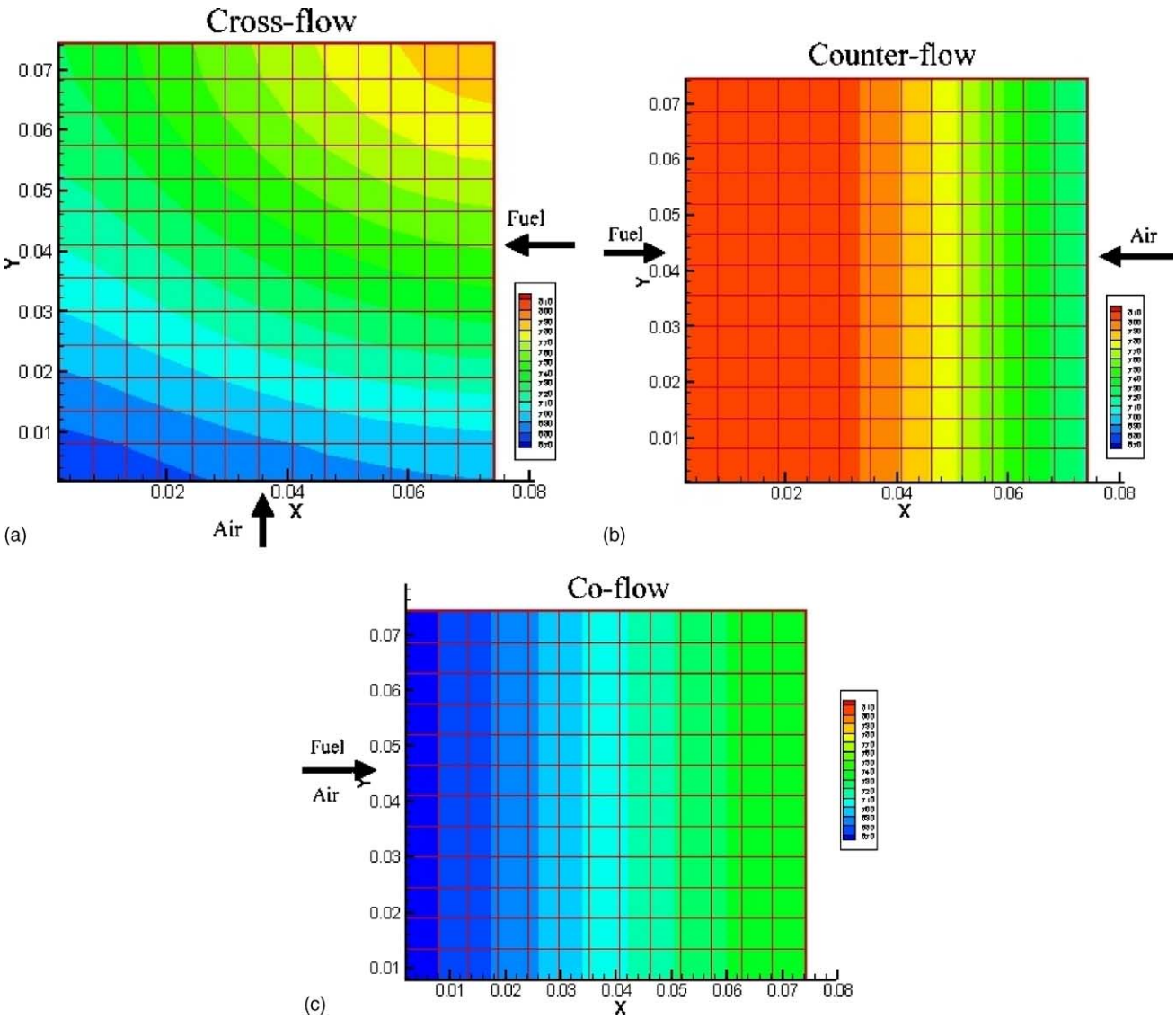

Fig. 8. (a) Temperature pattern of cross-flow cell with adiabatic boundaries. (b) Temperature pattern of counter-flow cell with adiabatic boundaries. (c) Temperature pattern of co-flow cell with adiabatic boundaries.

project specifications. The resulting steady-state average and maximum solid temperatures from the model computation are 773 and 802 °C, respectively. Fuel utilization is 66.5%, while the air consumption rate is at a minimal level of below 10% due to a relatively high value of the oxygen to water ratio ($\lambda \approx 7$). The input and output data are summarized in Table 1 for further reference.

The corresponding temperature distribution in the reaction zone is presented in Fig. 9. The distributions of fluid temperatures exhibit similar patterns, while the levels are slightly different. Near the fuel inlet, the maximum values of T_s, T_f and T_a are 802.4, 806.3 and 800.6 °C, respectively. The value of T_a at the air inlet is, however, somewhat lower than the others; the minimum values of T_s, T_f and T_a are 716.9, 721.6 and 680.3 °C, respectively. It should be noted that the temperature pattern shown in Fig. 9 is the outcome of the integrated electrochemical and heat transfer analyses illustrated in this work, which relieve the constraint of an adiabatic boundary condition at the edges of the reaction zone. On comparing the results in Fig. 9 with those in Fig. 8b, it is observed that the adiabatic boundaries impose a certain influence on the temperature distribution at the edges of the active area. By contrast, however, the central region remains almost unaffected, as far as the contour patterns are concerned. This outcome confirms the statement mentioned in the previous section. In addition, it will be shown later in this paper that the temperature level will be somewhat lower in the former case, due to the overall heat loss.

The overall cell characteristics are presented in Fig. 10. As reported in various studies, the value of 0.7 V has been selected as the operating voltage of a single cell for comparison purposes. The data yield 630 mA cm^{-2} and

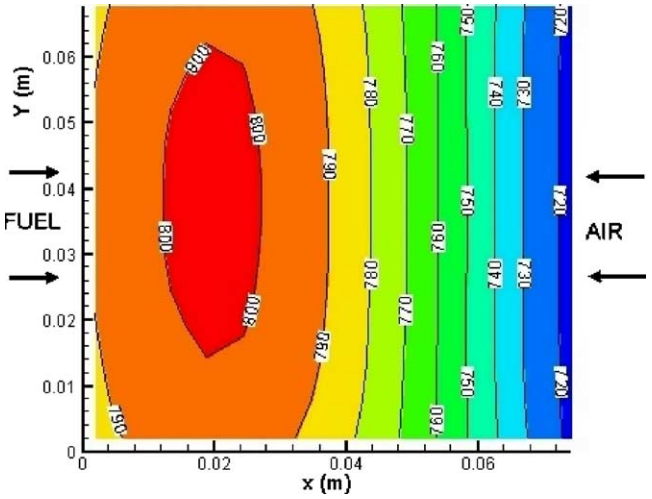

Fig. 9. Temperature distribution in cell.

440 mW cm^{-2} for the current density and the power density, respectively.

5.2. Thermal characteristics of the interconnect

Due to the symmetric nature of the present design, only half of the interconnect has been simulated in the analysis model; the other half can be presented as the mirror image. As mentioned above, a unified temperature distribution from both the electrochemical and finite element analyses can be obtained after several iterations, which will be shown in this section. Global temperature data of the finite element model for the interconnect with a two-layered insulation envelope are given in Fig. 11. It is seen that steep temperature gradients exist across the ceramic layers, which confirms the function of the insulation. In general, the outer temperature of the insulation envelope adjacent to the atmosphere can be reduced to values below 200 °C, depending on the material properties and thickness of the multi-layers. Compared with

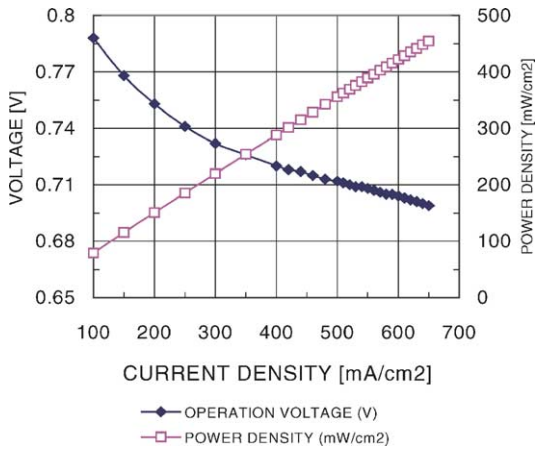

Fig. 10. SOFC characteristics.

the SOFC operating temperature of around 800 °C in the active area, lower temperatures of this level can substantially mitigate the amount of heat loss to the environment. Nevertheless, layout or optimization of stack insulation is subject to engineering practice.

Further insights of the thermal characteristics can be revealed by examining the FEA results for the interconnect itself, as presented in Fig. 12. In addition, the heat flux distribution at the periphery of the active area as well as the value of the heat loss per unit cell can be calculated by the FEA. Information about the heat flux distribution of the computation domain, i.e., upper half of the interconnect shown in Fig. 12, is presented in Table 2. It is observed that heat flux normal to the flow channels, q_y, varies from positive values near the fuel inlet to negative values towards the air inlet. This phenomenon shows a generic pattern in the active area with parallel-flow arrangements, i.e., the lateral heat flux is outwards near the fuel inlet side, but turns inwards on approaching the air inlet region. The heat flux parallel to the flow channels, q_x, is negative at the fuel inlet but positive at the opposite edge, which means that both the fuel and the air flow encounter upward temperature gradients along their individual flow direction for the counter-flow configuration. In summary, the results indicate two major features: (i) heat generation due to chemical reactions is most intense near the fuel inlet; and (ii) airflow is most effective at cooling near the air inlet.

5.3. Computational aspects

As described in Section 3.1, two-layered insulation materials, with an aim to reduce the heat loss to the environment, enclosed the SOFC unit. Three different insulation envelopes have been implemented in this work to investigate the heat transfer behaviour of a metallic interconnect with a ceramic enclosure. The inner layer of ceramic fibre was kept the same thickness of 10 mm, while three different values of 50, 75 and 100 mm were selected for the outer plate. These cases are identified here as A, B and C, respectively. Furthermore, it should be noted that case B is the basic configuration illustrated in Fig. 12. The temperature differences (ΔT) between the results from ECM and FEA for various insulation arrangements are presented in Fig. 13a–c. It is seen that the value of ΔT falls to less than 1 °C from a bulk value around 1000 °K on the interconnect, after three iterations. This outcome indicates that an accuracy of better than 0.1% has been achieved for all three cases. Hence, it has been confirmed that the convergent rate of the iteration process is very efficient.

For reference purposes, the computational resources required for the analyses are given here. The electrochemical calculations were performed on a Sun Ultra2 workstation, with 167 MHz CPU and 128 MB RAM, and the CPU time was around 1.5 h for each primary analysis. For subsequent iterations, much less computational efforts were required. For example, the CPU time for the first three iterations turned out to be around 3, 2.5 and 2 min, respectively. Alternatively, the

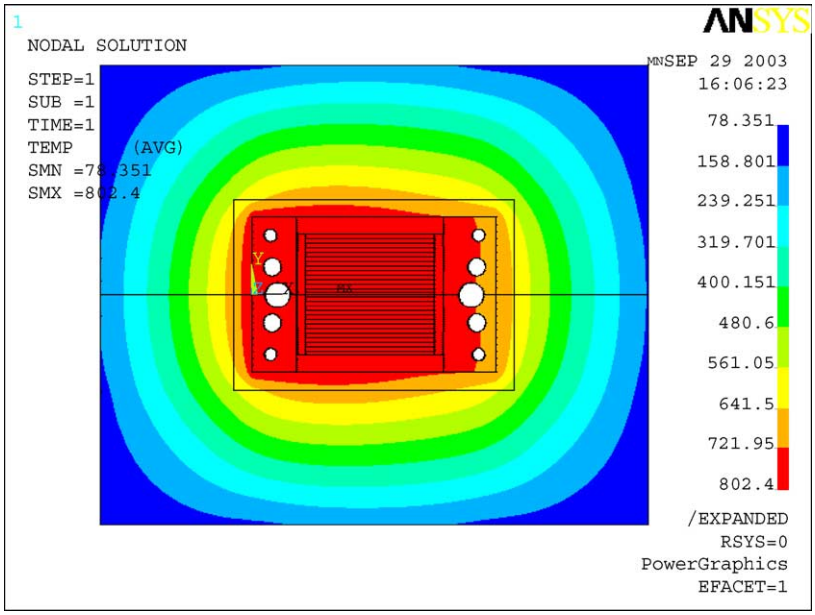

Fig. 11. Temperature distribution of interconnect including insulation.

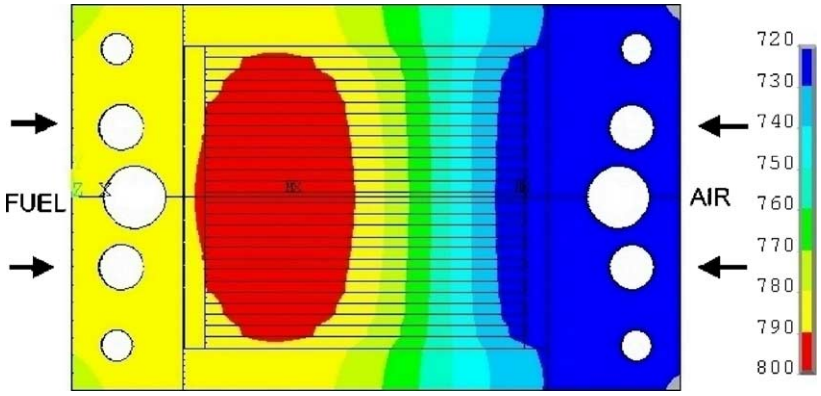

Fig. 12. Temperature distribution on interconnect.

Table 2
Heat flux on interconnect boundary

	Item													
	1	2	3	4	5	6	7	8	9	10	11	12	13	14
At upper periphery (kW m^{-2})														
x (mm)	1.93	7.85	13.35	18.85	24.35	29.85	35.35	40.85	46.35	51.85	57.35	62.85	68.35	74.28
q_y	3.37	5.13	6.5	7.54	8.1	8.05	7.28	5.74	3.51	0.8	−1.96	−4.16	−4.89	−2.64

	On the fuel inlet (left) side (kW m^{-2})							On the air inlet (right) side (kW m^{-2})						
	8[a]	9[a]	10[a]	11[a]	12[a]	13[a]	14[a]	8[a]	9[a]	10[a]	11[a]	12[a]	13[a]	14[a]
y (mm)	40.85	46.35	51.85	57.35	62.85	68.35	74.28	40.85	46.35	51.85	57.35	62.85	68.35	74.28
q_x	−2.91	−4.33	−4.47	−4.35	−4.15	−3.79	−3.46	3.66	0.97	0.54	0.56	0.57	0.55	0.37

[a] Item.

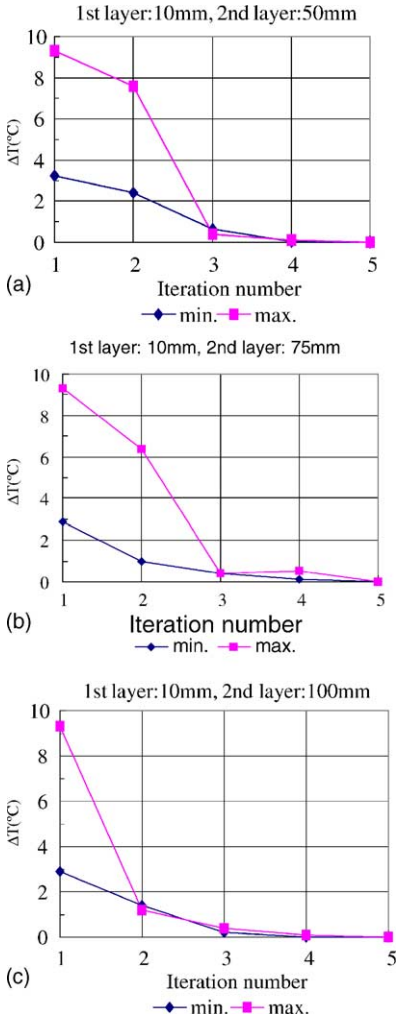

Fig. 13. (a) Convergent rate of iterations: case A. (b) Convergent rate of iterations: case B.

platform for FEA was a PENTIUM IV, 32-bit CPU 3.06 GHz, RAM 768 MB, and each computation needed a CPU time of slightly more than 2 min.

5.4. Parameter sensitivities

As described in Section 4, simplified design analysis tools would be favourable in the prototyping process, i.e., for providing a preliminary database of related components as well as for efficient parametric studies. Hence, the sensitivities of various thermal and flow parameters would be of major concern in identifying the predominant governing mechanisms.

5.4.1. Heat resistance

From Eq. (15), it is noted that the heat transfer behaviour from cell to environment is governed mainly by the following eight parameters: h_i, k_1, k_2, k_3, h_o, Δx_1, Δx_2 and Δx_3. The total heat resistance, $\sum R$, consists of five entities: (1) $R_1 = \Delta x_1/k_1$, (2) $R_2 = \Delta x_2/k_2$, (3) $R_3 = \Delta x_3/k_3$, (4) $R_i = 1/h_i$ and (5) $R_o = 1/h_o$. The first three items represent the resistances due to conduction in various materials, while the latter two are the counterparts from convection. The basic configuration mentioned above, i.e., case B, has been adopted here as a paradigm to illustrate the relative influence of the various heat resistances. For appropriate boundary conditions, the temperature of hot gas within the cell and surrounding atmosphere is assumed to be 800 and 40 °C, respectively. In the reference case for lateral heat flux at the periphery of the cell, Eq. (19) was implemented to evaluate the heat-transfer coefficient with internal forced convection, i.e., h_i. Nevertheless, other correlations will be discussed as well in a later section of this paper. In addition, the thickness between the outermost flow passage to the edge of interconnect was selected as the value for the channel wall, as a conservative measure for the resistance to heat conduction in the metal.

All the aforementioned geometric, material, thermal and flow parameters are summarized in Table 3 for easy reference. Calculated values of the heat resistances are also given. It is seen that the heat resistance of the outer insulation layer, R_3, assumes the highest value for the present configuration. Hence, the predominant parameters to affect the heat-transfer behaviour should be the thickness and material property of the ceramic plate used for insulation. This outcome also confirms the adequacy of applying an insulation envelope to enclose the SOFC unit, for reducing heat loss to the environment.

5.4.2. 1D heat-transfer results

Parametric studies with the 1D bulk model for design analysis described in Section 4 have been performed to investigate the influence of insulation layer thickness as well as heat-transfer coefficient. The test matrix of 1D analyses covered the combination of four different values of Δx_3 and various correlations of h_i. The data obtained from the simplified approach were then compared with the counterparts of FEM reported in Section 5.2, and empirical correlations could be deduced as the 'accommodation (rule-of-thumb) factors' for rapid prototyping purposes.

Referring to Fig. 11, the global 2D temperature distribution shows a pattern similar to that of a 'rectangular duct' enclosed by insulation materials. Hence, the concept of an

Table 3
Parameters of one-dimensional heat transfer

Geometry (mm)					
Δx_1	Δx_2	Δx_3	L	H	W
9	10	75	76	1	3

Thermal conductivity ($W m^{-1} °C^{-1}$)			Heat transfer coefficients ($W m^{-1} °C^{-1}$)	
k_1	k_2	k_3	h_i	h_o
25	0.198	0.215	154.6	9.88

Heat transfer resistance ($m^2 °C W^{-1}$)				
$R_1 = \Delta x_1/k_1$	$R_2 = \Delta x_2/k_2$	$R_3 = \Delta x_3/k_3$	$R_i = 1/h_i$	$R_o = 1/h_o$
0.00017	0.051	0.349	0.0065	0.101

Table 4
Results of one-dimensional heat transfer

Δx_3 (cm)	T_{w1} (°C)	T_{w2} (°C)	T_{w3} (°C)	T_{w4} (°C)	q (kW m^{-2})
h_i = 11.85 W m^{-2} °C^{-1} (plate), Nu_m = 11.5, L = 76 mm					
2.5	618.2	617.4	508.6	258.1	2.15
5.0	663.3	662.7	580.8	204.0	1.62
7.5	690.4	690.0	624.4	171.4	1.30
10	708.6	708.2	653.5	149.6	1.08
h_i = 4.46 W m^{-2} °C^{-1} (adiabatic, plate), Nu_1 = 5.385, L = 76 mm					
2.5	454.1	453.5	375.6	196.2	1.54
5.0	520.1	519.7	456.6	166.3	1.25
7.5	565.0	564.6	511.7	146.1	1.05
10	597.5	597.2	551.5	131.4	0.90
h_i = 154.6 W m^{-2} °C^{-1} (channel), Nu_2 = 3.68, D_h = 1.5 mm					
2.5	782.1	781.1	641.5	319.9	2.77
5.0	787.4	786.7	688.6	236.7	1.94
7.5	790.3	789.8	714.1	191.6	1.50
10	792.1	791.7	730.1	163.3	1.22

Thermal boundary conditions: T_{max} = 800 °C, T_o = 40 °C, h_o = 9.88 W m^{-2} °C^{-1}.

'outer critical insulation radius (r_{oc})' might apply for checking the suitability of the insulation thickness, provided that an effective diameter of the 'rectangular duct' can be deduced and can replace the diameter of a circular tube in a conventional approach. As given in textbooks, e.g. [18], the r_{oc} for a tube is a function of the thermal conductivity of the insulation material, k_i, and the heat-transfer coefficient at the outer boundary, h_o, and can be expressed as follows:

$$r_{oc} = \frac{k_i}{h_o} \tag{23}$$

On inserting the values of k_3 and h_o into Eq. (23), r_{oc} is found to be around 22 mm. This outcome indicates that the critical insulation diameter ($2 \times r_{oc}$) is smaller than the dimensions of the interconnect. Therefore, the physical configuration in this work has already gone beyond the regime of critical insulation, and heat loss should diminish with increasing thickness of the insulation.

The results obtained from the 1D bulk heat-transfer analyses are summarized in Table 4, in which wall temperatures and heat flux are listed against Δx_3 and h_i. For convenience, the related data extracted from cases A, B and C mentioned above are also presented in Table 5 for comparison with the counterparts from 1D analysis for lateral heat flux. Some selected data from Tables 4 and 5 are presented in graphical forms for easier illustration and interpretation. In engineering practice, the heat loss to the environment and the outer material temperature of the insulation envelope are of major concern and are shown in Figs. 14 and 15, respectively.

Table 5
Summary of 2D FEA results

Δx_3 (cm)	T_{w4} (°C)	q (kW m^{-2}), top	q (kW m^{-2}), right	q (kW m^{-2}), left
Two-dimensional heat transfer				
5.0	177.5	3.36	1.67	−4.70
7.5	144.7	2.89	0.97	−4.04
10	121.7	2.62	0.46	−3.63

ECM: h_i = 203.5 W m^{-2} °C^{-1}, k_f = 0.0763 W m^{-1} °C^{-1}, Nu = 4, D_h = 1.5 mm. FEA: k_1 = 25 W m^{-1} °C^{-1}, Δx_2 = 1 cm, k_2 = 0.198 W m^{-1} °C^{-1}, k_3 = 0.215 W m^{-1} °C^{-1}, h_o = 9.88 W m^{-2} °C^{-1}, T_o = 40 °C.

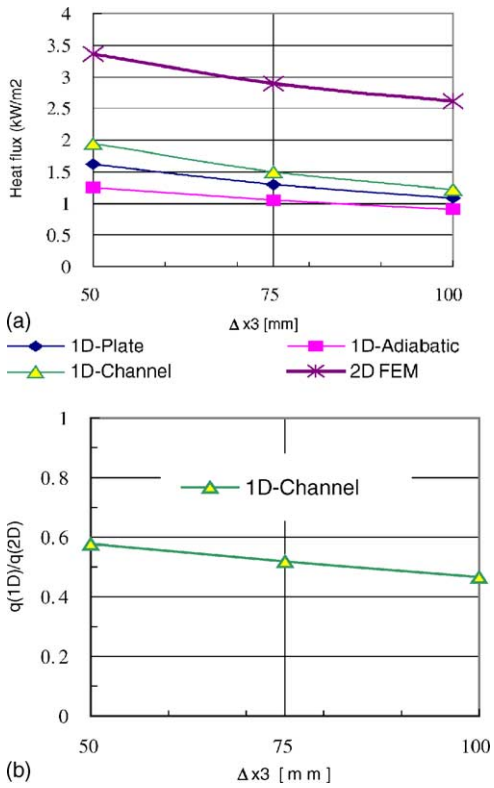

Fig. 14. (a) Heat flux vs. insulation thickness. (b) Relationship of lateral heat flux.

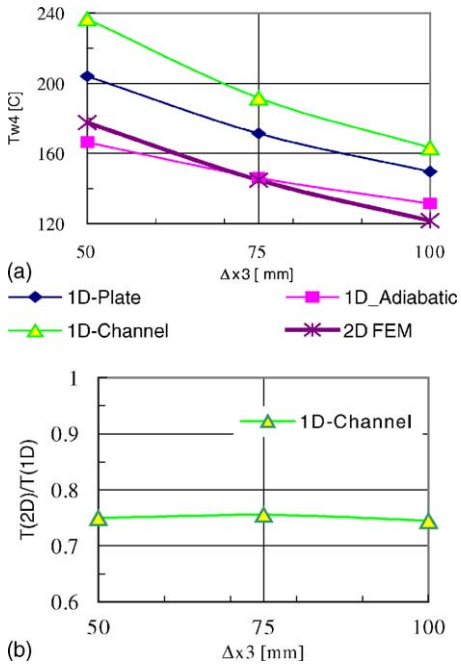

Fig. 15. (a) Outer material temperature vs. insulation thickness. (b) Relationship of material temperature.

The heat flux values of 1D calculations based on three different correlations as well as the lateral counterpart of the 2D FEA are shown in Fig. 14a. In general, the heat flux decreases with increasing thickness of the insulation layer, as expected. In addition, the variation of the heat-transfer coefficient for internal forced convection is somewhat neutralized by the larger heat resistances of the insulation materials; hence, the values of heat flux exhibit relatively minor changes among various 1D models. It should be noted that heat transfer over a flat plate, either in an open field or confined, mainly concerns the heat flux normal to the plate, which would be suitable for simulating the thermal behaviour on the end plates. The reason for presenting the results based on the correlations of $Nu_{m,i}$ and Nu_1 in Fig. 14a is two-fold: on the one hand, it shows the generic feature and capability of the model illustrated in Section 4; on the other hand, these data are required in later work to investigate the heat-transfer behaviour of the whole stack rather than a single cell. Geometrically, the flow channels on the interconnect are rectangular ducts. At present, this paper focuses on the heat-transfer phenomenon at the periphery of an SOFC; hence, the correlation of channel flow (i.e., Nu_2) would be more appropriate, although not identical to the present physical configuration, in establishing the simplified model for design analysis.

As illustrated in Fig. 12, the thermal characteristics of planar cells exhibit a 2D nature. Therefore, some 'accommodation factors' would be feasible to correlate the present 1D results with the counterparts of 2D FEA. The relationship between the lateral heat flux and the thickness of the insulation material is presented in Fig. 14b. The accommodation factor of heat flux, $AF_q = q(1D)/q(2D)$, is found to vary quasi-linearly within a range between 0.58 and 0.48, for Δx_3 increasing from 50 to 100 mm in the present investigation. This feature is quite promising from design analysis viewpoints. More parametric studies could be performed in the future to extend the comprehensiveness of the correlations, which would be beneficial to rapid prototyping processes.

Material temperatures at the outer boundary of insulation layer, T_{w4}, and the accommodation factor of the material temperature, $AF_T = T(2D)/T(1D)$, are shown in Fig. 15a and b, respectively. In general, AF_T exhibits a synergy with AF_q, but varies in the range between 0.75 and 0.74 in the present investigation.

6. Conclusions

This work presents efforts to establish integrated electrochemical and thermal analyses of a planar SOFC. The cell performance is evaluated by combining an electrochemical model with a simplified thermal approach, which can be implemented for various flow configurations. Based on 'quasi-conduction' procedures, a finite element model is employed to simulate the 2D heat-transfer behaviour on an interconnect with insulation envelopes. This calculates not only the temperature distribution, but also the heat flux dissipated to the environment. The latter then serves as a correction term to the ECM for refined evaluation of cell performance, so that a unified temperature distribution with a heat loss effect can be obtained via iteration processes.

It has been verified that a temperature accuracy of better than 0.1% can be achieved within a few iterations. In addition, this work relieves the constraint of thermal boundaries for the active area of SOFC, and realistically mimics the heat-transfer phenomenon at the periphery. By combining ECM with FEM, cost-intensive and time-consuming CFD efforts are circumvented, and consistent and synergetic thermal characteristics are generated. Hence, it can be concluded that an efficient computational methodology for integrated electrochemical and heat-transfer analyses has been accomplished, which will be utilized in the future to acquire the necessary design data for prototyping SOFC system applications.

A bulk heat-transfer model for simplified design analysis has also been developed. By implementing various empirical correlations from textbooks, the model can be utilized to study either normal or lateral heat transfer phenomena in a planar cell, of which the latter has been the major concern in this study. In engineering practice, insulation materials would be deployed as an enclosure for an SOFC stack to reduce heat loss to the environment. The concept of total heat resistance would then be employed to facilitate 1D heat-transfer analysis, and the relative magnitude of the resistance due to different heat-transfer mechanisms or material properties could be evaluated accordingly. Hence, predominant parameters that affect heat-transfer behaviour could be readily determined. Moreover, some 'accommodation factors' to correlate the 1D results with the counterparts of 2D FEA have been deduced from the presently available data. It is expected that more comprehensive correlations can be generated with extended parametric studies, which will be beneficial for providing rapid prototyping processes.

References

[1] E. Achenbach, J. Power Sources 49 (1994) 333–348.
[2] M. Iwata, T. Hikosaka, M. Morita, Solid State Ionics 132 (2000) 297–308.
[3] H. Yakabe, T. Ogiwara, I. Yasuda, M. Hishinuma, in: Proceedings of the Sixth International Symposium on Solid Oxide Fuel Cells, vol. 99 (19), 1999, pp. 1087–1098.
[4] H. Yakabe, T. Ogiwara, M. Hishinuma, I. Yasuda, J. Power Sources 102 (2001) 144–154.
[5] K.P. Recknagle, R.E. Williford, L.A. Chick, D.R. Rector, M.A. Khaleel, J. Power Sources 113 (2003) 109–114.
[6] Y.-P. Chyou, T.-D. Chung, J.-S. Chen, J.-J. Chen, in: Proceedings of 27th Conference on Theoretical and Applied Mechanics: Thermal, Fluid, and Solid Mechanics Series, Tainan, Taiwan, vol. I, 2003, pp. 176–183 (in Chinese).
[7] Y.-P. Chyou, T.-D. Chung, J.-S. Chen, R.-F. Shie, in: Proceedings of 6th European Solid Oxide Fuel Cell Forum, Lucerne, Switzerland, vol. 2, 2004, pp. 646–655.
[8] J.-S. Chen, Y.-P. Chyou, C.-C. Tzeng, S.-T. Chou, S.-H. Chen, Model Calculation for Planar Solid Oxide Fuel Cell, INER Research Report, INER-2495 (in Chinese), October 2003.

[9] J.R. Ferguson, J.M. Fiard, R. Herbin, J. Power Source 58 (1996) 109–122.
[10] S. Nagata, A. Momma, T. Kato, Y. Kasuya, J. Power Sources 101 (2001) 60–71.
[11] S.H. Chan, K.A. Khor, Z.T. Xia, J. Power Source 93 (2001) 130–140.
[12] H. Yakabe, M. Hishinuma, M. Uratani, Y. Matsuzaki, I. Yasuda, J. Power Sources 86 (2000) 423–431.
[13] M.W. Chase Jr., C.A. Davies, J.R. Downey Jr., D.J. Frurip, R.A. McDonald, A.N. Syverud, Joint Army–Navy–Air Force Thermochemical Tables, third ed., National Bureau of Standard, Washington, USA, 1985.
[14] J. Yuan, M. Rokni, B. Sundén, in: Proceedings of the Sixth International Symposium on Solid Oxide Fuel Cells, vol. 99 (19), 1999, pp. 1099–1108.
[15] W. Lehnert, J. Meusinger, F. Thom, J. Power Sources 87 (2000) 57–63.
[16] R.-F. Shie, J.-J. Chen, Thermal Stress Analysis of Interconnect of Solid Oxide Fuel Cells, ANSYS Taiwan User Conference (in Chinese), Yunlin, Taiwan, 2003.
[17] ANSYS, ANSYS User's Manual, Version 7.0, ©ANSYS, Inc., USA, 2003.
[18] M.N. Ozisik, Heat Transfer—A Basic Approach, McGraw-Hill, New York, 1985, pp. 294–295.